Three-Dimensional Solution Structure of μ-Conotoxin GIIIB, a Specific Blocker of Skeletal Muscle Sodium Channels[†,‡]

Justine M. Hill, Paul F. Alewood, and David J. Craik*

Centre for Drug Design and Development, University of Queensland, Brisbane, Queensland 4072, Australia

Received January 11, 1996; Revised Manuscript Received April 22, 1996[⊗]

ABSTRACT: The three-dimensional solution structure of μ-conotoxin GIIIB, a 22-residue polypeptide from the venom of the piscivorous cone snail *Conus geographus*, has been determined using 2D ^{1}H NMR spectroscopy. GIIIB binds with high affinity and selectivity to skeletal muscle sodium channels and is a valuable tool for characterizing both the structure and function of these channels. Structural restraints consisting of 289 interproton distances inferred from NOEs and 9 backbone and 5 side chain dihedral angle restraints from spin−spin coupling constants were used as input for simulated annealing calculations and energy minimization in the program X-PLOR. In addition to the ^{1}H NMR derived information, the ^{13}C resonances of GIIIB were assigned at natural abundance, and hydroxyproline Cβ and Cγ chemical shifts were used to distinguish between the *cis* and *trans* peptide bond conformations. The final set of 20 structures had mean pairwise rms differences over the whole molecule of 1.22 Å for the backbone atoms and 2.48 Å for all heavy atoms. For the well-defined region encompassing residues 3−21, the corresponding values were 0.74 and 2.54 Å, respectively. GIIIB adopts a compact structure consisting of a distorted 3_{10}-helix, a small β-hairpin, a *cis*-hydroxyproline, and several turns. The molecule is stabilized by three disulfide bonds, two of which connect the helix and the β-sheet, forming a structural core with similarities to the CS$\alpha\beta$ motif [Cornet, B., Bonmatin, J.-M., Hetru, C., Hoffmann, J. A., Ptak, M., & Vovelle, F. (1995) *Structure 3*, 435−448]. This motif is common to several families of small proteins including scorpion toxins and insect defensins. Other structural features of GIIIB include the presence of eight arginine and lysine side chains that project into the solvent in a radial orientation relative to the core of the molecule. These cationic side chains form potential sites of interaction with anionic sites on sodium channels. The global fold is similar to that reported for μ-conotoxin GIIIA, and the structure of GIIIB determined in this study provides the basis for further understanding of the structure−activity relationships of the μ-conotoxins and for their binding to skeletal muscle sodium channels.

Voltage-dependent sodium channels mediate changes in sodium permeability across the membranes of electrically excitable cells. The primary structure of a number of subtypes of these channels from various tissues and species has been identified (Kallen et al., 1993, and references therein). A large number of neurotoxins including tetrodotoxin, batrachotoxin, α- and β-scorpion toxins, and ciguatoxins bind with high affinity and specificity to the sodium channels at six or more sites. These neurotoxins provide specific probes for distinct regions of the sodium channels, greatly facilitating the study of their functional and structural properties [for reviews see Strichartz et al. (1987) and Catterall (1988, 1995)].

Peptide toxins from *Conus* snail venoms are valuable research tools in many fields of neurobiology since they provide high-affinity antagonists for voltage-gated ion channels (sodium, calcium) and ligand-gated receptors (acetylcholine, NMDA)[1] in excitable tissues (Myers et al., 1993; Olivera et al., 1990, 1991). The μ-conotoxins, from the piscivorous cone snail *Conus geographus*, are a family of 22-residue polypeptides containing three hydroxyproline residues and three intramolecular disulfide bonds (Sato et al., 1983; Cruz et al., 1985; Hidaka et al., 1990) as shown in Figure 1. These toxins specifically block skeletal muscle sodium channels (Cruz et al., 1985; Moczydlowski et al., 1986). By contrast, classical sodium channel blockers tetrodotoxin (TTX) and saxitoxin (STX) block neuronal sodium channels as well as muscle sodium channels.

Sodium channel blockers such as the μ-conotoxins serve as molecular markers and specific probes of the pore region of the channel. Identification of the segments which line the transmembrane pore and define the conductance and ion selectivity of the channels is of great interest and importance

[†] This work was supported in part by a grant from the Australian Research Council (D.J.C.) and an Australian Postgraduate Award (J.M.H.).

[‡] Coordinates of the final structures have been deposited at the Brookhaven Protein Data Bank, Upton, NY 11973, under the accession code 1GIB.

* To whom correspondence should be addressed. Fax: +61-7-3365-2487. Phone: +61-7-3365-4945.

[⊗] Abstract published in *Advance ACS Abstracts,* June 15, 1996.

[1] Abbreviations: GIIIA(B), μ-conotoxin GIIIA(B) from *Conus geographus*; TTX, tetrodotoxin; STX, saxitoxin; NMDA, *N*-methyl-D-aspartate; Hyp (O), 4-*trans*-L-hydroxyproline; Boc, *tert*-butoxycarbonyl; HPLC, high-performance liquid chromatography; 1D, one dimensional; 2D, two dimensional; NMR, nuclear magnetic resonance; DQF-COSY, double-quantum-filtered 2D correlation spectroscopy; E-COSY, exclusive COSY; TOCSY, 2D total correlation spectroscopy; NOE, nuclear Overhauser effect; NOESY, 2D NOE spectroscopy; HMQC, 2D heteronuclear multiple-quantum coherence spectroscopy; WATERGATE, water suppression by gradient-tailored excitation; DSS, 4,4-dimethyl-4-silapentane-1-sulfonate; rms, root mean square; CS$\alpha\beta$, cysteine-stabilized $\alpha\beta$; CSH, cysteine-stabilized α-helical.

S0006-2960(96)00073-6 CCC: $12.00

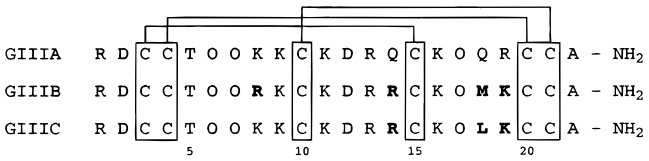

FIGURE 1: Amino acid sequences and disulfide bonds of μ-conotoxins GIIIA, GIIIB, and GIIIC from *C. geographus* (O = 4-*trans*-L-hydroxyproline). Residues that differ in sequence from GIIIA are highlighted in bold type.

(Catterall, 1995). The μ-conotoxins bind competitively with TTX and STX for site 1; however, recent mutagenesis studies suggest that they have distinct attachment sites (Stephan et al., 1994). The high affinity and selectivity of μ-conotoxins for skeletal muscle sodium channels make them valuable for characterizing both the structure and function of these channels and for probing variability in sodium channel structures.

Investigation of the three-dimensional structure of GIIIA by 2D ^{1}H NMR spectroscopy (Lancelin et al., 1991; Ott et al., 1991; Wakamatsu et al., 1992) has shown that the overall shape is that of a disk $\sim$6 $\times$ 15 Å for the backbone, from which seven arginine and lysine side chains project radially into the solvent. The important residues for activity (Arg13, Lys16, Hyp17, and Arg19) are clustered on one side of the molecule, suggesting that this face associates with the receptor site (Wakamatsu et al., 1992). Detailed information on the conformation of other μ-conotoxins is necessary for defining sites that interact with the sodium channels and for probing the molecular arrangement of the skeletal muscle sodium channel. This paper describes the three-dimensional structure of GIIIB in aqueous solution, as determined using 2D ^{1}H NMR spectroscopy. GIIIB differs from GIIIA at four positions as illustrated in Figure 1, with the net result being the presence of one more positive charge in GIIIB. It has been suggested that the guanidino group at residue 14 in GIIIB may be responsible for its enhanced toxicity over GIIIA (Sato et al., 1983), and it is of interest to determine if the amino acid substitutions from GIIIA have a significant effect on the conformation. The structure of GIIIB determined in this study provides the basis for further understanding of the structure−activity relationships of the μ-conotoxins and for their binding to skeletal muscle sodium channels. Structural similarities with other polypeptides are also discussed.

EXPERIMENTAL PROCEDURES

Materials. GIIIB was prepared by Boc chemistry solid-phase peptide synthesis, and the disulfide bonds were formed by air oxidation (Hill et al., to be published elsewhere). Analytical reverse-phase HPLC and electrospray mass spectrometry confirmed the purity and molecular weight of the synthetic peptide. Coinjection of equal amounts of synthetic and natural GIIIB resulted in a single symmetrical peak which eluted with a retention time identical with times determined for the individual peptides. D_2O (99.9% and 99.99%) was obtained from Cambridge Isotope Laboratories, Woburn, MA.

NMR Spectroscopy. Samples for ^{1}H NMR measurements contained 3 mM peptide in either 99.99% D_2O or 90% H_2O/10% D_2O (v/v) at pH 3.5. Spectra were recorded at 10 and 25 °C on a Bruker ARX-500 spectrometer equipped with a shielded gradient unit. Low-temperature studies employed a temperature-controlled stream of cooled air using a Bruker BCU refrigeration unit and a B-VT 2000 control unit. 2D NMR spectra were recorded in phase-sensitive mode using time-proportional phase incrementation for quadrature detection in the t_1 dimension (Marion & Wüthrich, 1983). The 2D experiments included DQF-COSY (Rance et al., 1983), E-COSY (Griesinger et al., 1987), TOCSY (Braunschweiler & Ernst, 1983) using a MLEV-17 spin lock sequence (Bax & Davis, 1985) with a mixing time of 80 ms, and NOESY (Jeener et al., 1979) with mixing times of 100, 250, and 350 ms. For DQF-COSY and E-COSY experiments, solvent suppression was achieved using selective low-power irradiation of the water resonance during a relaxation delay of 1.8 s. Solvent suppression for NOESY and TOCSY experiments was achieved using a modified WATERGATE sequence (Piotto et al., 1992) in which two gradient pulses of 2 ms duration and 6 G cm^{-1} strength were applied on either side of a binomial 3−9−19 pulse. Spectra were routinely acquired over 6024 Hz with 4096 complex data points in F_2 and 400−600 increments in the F_1 dimension, with 32 scans per increment (64 for NOESY). Slowly exchanging NH protons were detected by acquiring a series of 1D and TOCSY spectra of the fully protonated peptide immediately following dissolution in D_2O. $^3J_{H\alpha-H\beta}$ coupling constants were measured from E-COSY spectra, and $^3J_{NH-H\alpha}$ coupling constants were measured from DQF-COSY spectra, strip-transformed to 8K $\times$ 1K. 1D slices from this spectrum were analyzed using a simple peak simulation routine to obtain approximate coupling constants.

^{1}H−^{13}C HMQC (Bax et al., 1983) and HMQC-TOCSY (Lerner & Bax, 1986) spectra were recorded for a 13 mM peptide sample in 99.99% D_2O. Spectral widths in the ^{1}H and ^{13}C dimensions were 5050 and 12577 Hz, respectively, and 4096 complex data points were acquired with 256 F_1 increments. The ^{13}C HMQC spectrum was accumulated with 32 scans per increment and 128 scans for the ^{13}C HMQC-TOCSY spectrum.

Spectra were processed on a Silicon Graphics Indigo workstation using UXNMR (Bruker) and FELIX (Biosym Technologies, San Diego, CA) software. The t_1 dimension was zero-filled to 2048 real data points, and 90° phase-shifted sine bell window functions were applied prior to Fourier transformation. Spectra were referenced to external 4,4-dimethyl-4-silapentane-1-sulfonate (DSS).

Structural Restraints. Distance restraints were derived primarily from the 250 ms NOESY spectrum recorded at 10 °C. A small number of restraints were also derived from spectra recorded at 10 °C, 350 ms and 25 °C, 250 ms. Peak volumes were classified as strong, medium, or weak, corresponding to upper bound interproton distance restraints of 2.7, 3.5, and 5.0 Å, respectively (Williamson et al., 1985; Clore et al., 1986a). Peaks that were observed only in the 350 ms spectrum were classified as very weak and assigned to an upper bound distance restraint of 6.0 Å. Appropriate pseudoatom corrections were applied to nonstereospecifically assigned methylene and methyl protons (Wüthrich et al., 1983). Backbone dihedral restraints were inferred from $^3J_{NH-H\alpha}$ coupling constants, with ϕ restrained to $-120 \pm 40°$ for a $^3J_{NH-H\alpha}$ greater than 8 Hz and to $-65 \pm 25°$ for a $^3J_{NH-H\alpha}$ less than 5 Hz (Pardi et al., 1984). Several side chain χ^1 angles were restrained on the basis of observed NOE

and $^3J_{H\alpha-H\beta}$ coupling patterns. A t^2g^3 side chain conformation restrained the χ^1 angle to $-60 \pm 30°$ and a g^2g^3 conformation to $+60 \pm 30°$ (Wagner et al., 1987).

Structure Calculations. Three-dimensional structures were calculated using a simulated annealing and energy minimization protocol in the program X-PLOR 3.1 (Brünger, 1992). In the first step an *ab initio* simulated annealing protocol (Nilges et al., 1988) was used, starting from template structures with randomized ϕ and ψ angles and extended side chains, to generate a set of 20 structures. At this stage the disulfide bonds were included as pseudo-NOE restraints, and the simulated annealing protocol consisted of 20 ps of high-temperature molecular dynamics (1000 K) with a low weighting on the repel force constant and NOE restraints. This was followed for a further 10 ps with an increased force constant on the experimental NOE restraints. The disulfide bonds were then formally included, and the dihedral force constant was increased prior to cooling the system to 300 K and increasing the repel force constant over 15 ps of dynamics.

The NOE restraints were checked for violations, and ambiguous cross peaks were resolved on the basis of interproton distances in the initial family of structures. A further 50 structures were calculated with the inclusion of ϕ and χ^1 dihedral angle restraints derived from spin−spin coupling constants and tightened distance restraints involving stereospecifically assigned protons that had been given pseudoatom status in the initial calculations. Refinement of these structures was achieved using the conjugate gradient Powell algorithm with 1000 cycles of energy minimization (Clore et al., 1986b) and a refined force field based on the program CHARMm (Brooks et al., 1983). The C-terminal amide group was excluded from the calculations as no medium- or long-range NOEs were observed for this part of the molecule. ω angles were set to *trans* with the exception of Hyp6−Hyp7, which was set to the *cis* configuration. Structures were analyzed using SSTRUC (D. Smith, unpublished program), based on the algorithm of Kabsch and Sander (1983), and displayed using INSIGHT (Biosym Technologies, San Diego, CA).

RESULTS

^{1}H Resonance Assignments. Sequence-specific resonance assignment of GIIIB was achieved using well-established techniques (Wüthrich, 1986). Any ambiguities due to peak overlap with the water resonance or chemical shift degeneracy were resolved by comparison of TOCSY and NOESY spectra recorded at 10 and 25 °C. The first step in resonance assignment, i.e., identification of the individual spin systems and assignment to amino acid type, is illustrated by the TOCSY spectrum in Figure 2A. This shows connectivities from backbone amide and several side chain NH resonances. The behavior of the amide NH proton of Cys10 was temperature dependent. At 25 °C the resonance was extremely broad; however, at 10 °C it sharpened and gave rise to visible cross peaks. This broadening of the resonance at higher temperature has previously been observed for Cys10 in the related peptides GIIIA and [Ala^{13}]GIIIA (Lancelin et al., 1991; Wakamatsu et al., 1992), when it was suggested to be due to chemical exchange between two or more different states.

The second step in the assignment process was to align the spin systems according to the primary structure of GIIIB

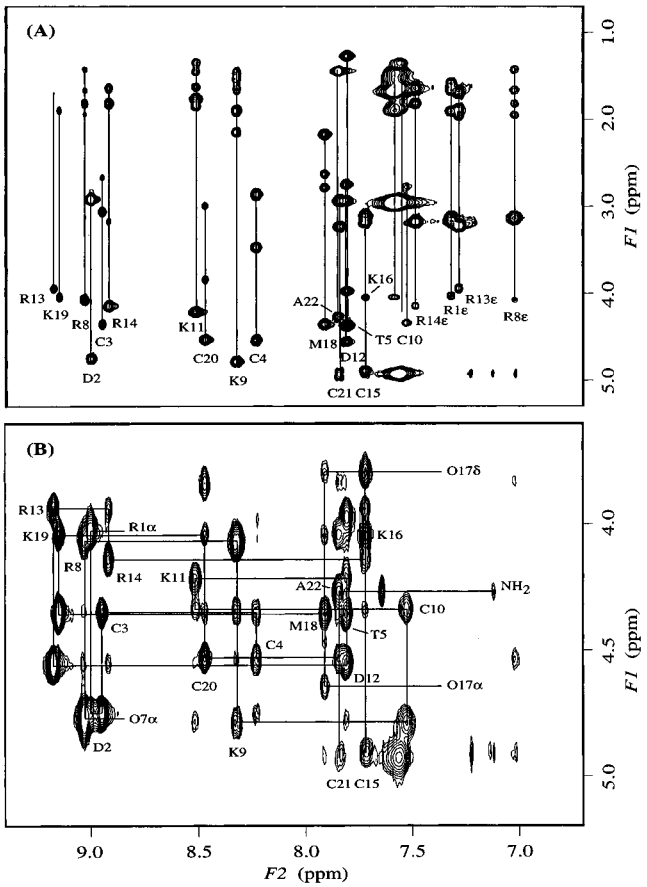

FIGURE 2: Regions of (A) 80 ms TOCSY and (B) 250 ms NOESY spectra of 3 mM GIIIB in 90% H_2O/10% D_2O at 10 °C, pH 3.5. In the TOCSY spectrum, connectivities from lysine side chain NH resonances are not labeled for clarity. In the NOESY spectrum, $H\alpha-NH_{i+1}$ connectivities are shown for residues 1−4, 7−15, and 17−21. Intraresidue NH−Hα cross peaks are marked with the one-letter code for the amino acid and residue number.

using sequential connectivities in the NOESY spectrum. The fingerprint region of the NOESY spectrum illustrating the $H\alpha-NH_{i+1}$ connectivities is shown in Figure 2B. For hydroxyproline residues, either $H\alpha-H\delta_{i+1}$ or $H\alpha-H\alpha_{i+1}$ connectivities were used instead of $H\alpha-NH_{i+1}$. The sequential assignment was supported by $NH-NH_{i+1}$ and $H\beta-NH_{i+1}$ NOE connectivities as summarized in Figure 3.

Stereospecific assignments of several nonequivalent AMX Hβ protons were made by identifying the classical staggered χ^1 conformations through analysis of $^3J_{H\alpha-H\beta}$ coupling constants determined from E-COSY spectra and the strength of Hα−Hβ and NH−Hβ intraresidue NOEs in the 100 ms NOESY spectrum (Wagner et al., 1987; Hyberts et al., 1987). Stereospecific assignments were determined for cysteine residues 3, 4, 10, 20, and 21, and χ^1 restraints were obtained for residues 3, 4, 10, and 21 ($-60 \pm 30°$) and for residue 20 ($+60 \pm 30°$). The ^{1}H chemical shifts and stereospecific assignments of GIIIB are listed in the supporting information (Table S1).

^{13}C Resonance Assignments. ^{13}C chemical shifts were determined by combined analysis of proton-detected HMQC and HMQC-TOCSY spectra. Using the ^{1}H chemical shifts, and the fact that ^{13}C chemical shifts are located in characteristic regions of the spectrum depending on the carbon and residue types (Wüthrich, 1976; Howarth & Lilley, 1978), many of the resonances could be assigned unambiguously in the HMQC spectrum. However, ^{1}H chemical shift

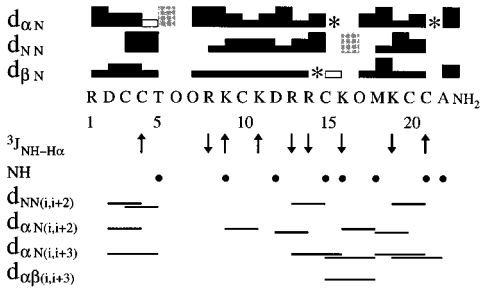

FIGURE 3: Summary of the sequential and medium-range NOE connectivities, $^3J_{NH-H\alpha}$ coupling constants, and slowly exchanging NH protons observed for GIIIB. Filled bars indicate sequential connectivities observed in a 250 ms NOESY spectrum at 10 °C, pH 3.5. Shaded bars correspond to sequential Hα−Hδ_{i+1} and NH−Hδ_{i+1} connectivities for hydroxyproline residues. Open bars indicate connectivities observed at 25 °C. The height of the bar indicates the strength of the NOE. Overlapping NOEs are indicated by an asterisk (*). ↓ indicate $^3J_{NH-H\alpha}$ coupling constants ≤ 5 Hz, ↑ indicate $^3J_{NH-H\alpha}$ coupling constants ≥8 Hz. Slowly exchanging backbone NH protons (observed in a TOCSY spectrum recorded in D_2O) are indicated by filled circles.

degeneracies prevented the unique determination of several ^{13}C resonances, and these were assigned using the HMQC-TOCSY spectrum. The aliphatic Cα−Hα region of the HMQC spectrum of GIIIB and the ^{13}C resonance assignments are available as supporting information (Figure S1 and Table S2, respectively).

Conformation of Hydroxyproline Residues. GIIIB contains three hydroxyproline residues, the conformation of which may be inferred from sequential NOE connectivities. As is the case for proline (Wüthrich, 1986), strong NOEs between the Hδ protons of Hyp and the Hα proton of the preceding residue indicate the presence of a *trans* peptide bond, whereas NOEs between the Hα proton of Hyp and the Hα proton of the preceding residue indicate the presence of a *cis* peptide bond. The conformations of the peptide bonds preceding Hyp6 and Hyp17 appear to be *trans*, based on the observation of strong Hα−Hδ_{i+1} and NH−Hδ_{i+1} connectivities, respectively. However, chemical shift degeneracy of the Hα protons of Hyp6 and Hyp7 at both 10 and 25 °C prevented the observation of either Hα−Hδ_{i+1} or Hα−Hα_{i+1} connectivities for Hyp7, so the conformation of the peptide bond could not be determined solely from NOE connectivities.

^{13}C chemical shifts provided useful additional information to establish the conformation of the Hyp6−Hyp7 peptide bond. The ^{13}C chemical shifts of hydroxyproline Cβ and Cγ distinguish between the two forms, as the Cβ (38−40 ppm for *trans* and 41−42 ppm for *cis*) and Cγ (71−72 ppm for *trans* and 70−71 ppm for *cis*) resonances are different (Garbay-Jaureguiberry et al., 1980). In GIIIB, the Cβ and Cγ resonances of Hyp6 and Hyp17 appear at 38.9 and 72.0−72.4 ppm (Table 1), respectively, suggesting these residues adopt the *trans* conformation in accordance with the NOE data. By contrast, the Cβ and Cγ resonances of Hyp7 appear at 40.6 and 70.5 ppm, respectively, indicative of a *cis* peptide bond.

Secondary Structure. A qualitative analysis of short- and medium-range NOEs, $^3J_{NH-H\alpha}$ coupling constants, and NH exchange rates (Wüthrich, 1986) was used to characterize the secondary structure of GIIIB. These data are summarized in Figure 3. The presence of helix from residues 13−22 is suggested by several weak Hα−NH$_{i+3}$ connectivities and a medium Hα-Hβ_{i+3} connectivity between Cys15 and Met18.

Table 1: ^{13}C Chemical Shifts (ppm) for the Hydroxyproline Residues of GIIIB at 10 °C, pH 3.5[a,b]

residue	Cα	Cβ	Cγ	Cδ	$\Delta\delta_{C\gamma-C\beta}$[c]
Hyp6	59.4	38.9	72.4	58.3	**33.5**
Hyp7	60.5	40.6	70.5	57.6	**29.9**
Hyp17	61.6	38.9	72.0	58.0	**33.1**

[a] ^{13}C chemical shifts are reported relative to the methyl resonance of external DSS at 0 ppm. [b] Complete ^{13}C resonance assignments of GIIIB are listed in the supporting information (Table S2). [c] A decreased ^{13}C chemical shift dispersion of Cγ and Cβ in a Hyp residue ($\Delta\delta_{C\gamma-C\beta}$ ∼ 30 ppm) suggests that the preceding carbonyl is configured in a *cis* peptide bond, while Hyp having a more common *trans* peptide bond shows greater chemical shift dispersion ($\Delta\delta_{C\gamma-C\beta}$ ∼ 33 ppm).

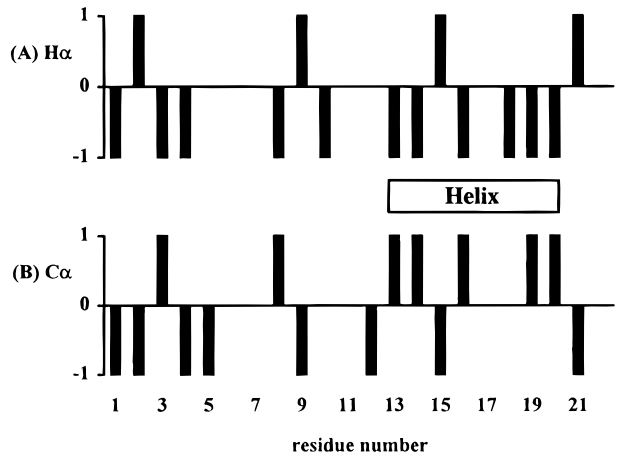

FIGURE 4: Chemical shift index derived from (A) Hα and (B) Cα chemical shifts of GIIIB. An index of −1 and +1 indicates a shift deviation from the random coil value of greater than 0.1 ppm (Hα) or 0.7 ppm (Cα) upfield and downfield, respectively, and those within the range of the random coil value are indicated by 0 (Wishart et al., 1992; Wishart & Sykes, 1994). A grouping of four or more successive −1 (Hα) or +1 (Cα) is often taken as evidence of helical conformation.

This is supported by the observation of slowly exchanging NH protons at positions 15, 16, 18, 21, and 22 and small $^3J_{NH-H\alpha}$ coupling constants (<5 Hz) at positions 13, 14, 16, and 19. However, the presence of Hα−NH$_{i+2}$ connectivities and absence of Hα−NH$_{i+4}$ connectivities over this region suggest that the 3_{10}-helix is the dominant folded form rather than the α-helix. Any helix present is likely to be distorted due to a hydroxyproline at position 17 and cysteine residues at positions 15, 20, and 21 which participate in disulfide bonds to other parts of the molecule. A large $^3J_{NH-H\alpha}$ coupling constant (>8 Hz) for Cys21 provides evidence for this distortion from standard geometry. Additional support for helix is provided by analysis of the Hα and Cα chemical shifts (Wishart et al., 1991, 1992; Wishart & Sykes, 1994). The Hα and Cα resonances of most residues in the sequence 13−22 showed characteristic helical shifts (upfield for Hα and downfield for Cα) from their random coil values as shown in Figure 4. The data also suggest some distortions in the helix at positions 15 and 21.

Two β-turns involving residues 2−5 and 9−12 were identified on the basis of characteristic NOE patterns and coupling constants. The slowly exchanging NH protons of residues 5 and 12 support the presence of tight turns which may tentatively be classified as type I. A short stretch of antiparallel β-sheet involving residues 3−4 and 8−9 is inferred from a number of long-range NOEs, including Hα−NH connectivities between residues 3, 9 and 4, 9 and a Hα−

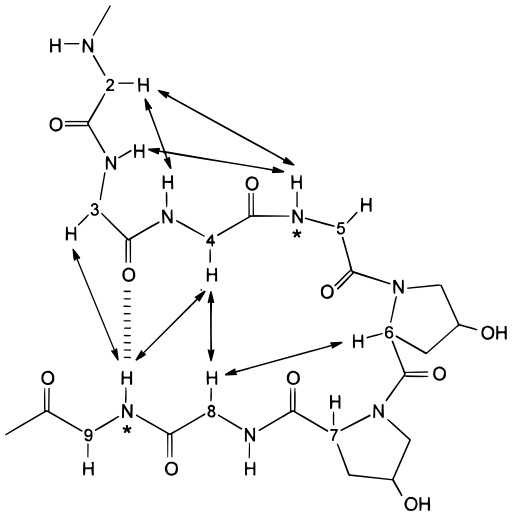

FIGURE 5: Schematic diagram of the β-hairpin region of GIIIB showing the interstrand NOEs (arrows), potential hydrogen bonds (broken lines), and slowly exchanging amide NH protons (*).

Hα connectivity between residues 4 and 8 as illustrated in Figure 5. This structural element is henceforth referred to as a β-hairpin, although it is important to emphasize that it is distorted relative to the classical β-hairpin conformations described by Sibanda et al. (1989). The presence of a β-hairpin structure is supported by the observation of large $^3J_{NH-H\alpha}$ coupling constants (>8 Hz) for residues 4 and 9 and a slowly exchanging NH at position 9. However, a coupling constant of <5 Hz for residue 8 suggests distortion in this region.

Disulfide Bonding Pattern. The synthetic GIIIB was observed to coelute with natural GIIIB on reverse-phase HPLC, suggesting that the native disulfide bonds had been formed. The NMR data also confirmed the disulfide pairings of the six cysteine residues in synthetic GIIIB. Long-range Hα−Hβ connectivities observed between Cys15 and Cys3 and between Cys10 and Cys21 and Hβ−Hβ connectivities between Cys3 and Cys15 and between Cys4 and Cys20 suggest the presence of disulfide bridges (Klaus et al., 1993) between 3−15, 4−20, and 10−21. This pattern of disulfide bridges was further verified by statistical analysis of the S−S distances in 20 structures calculated without the inclusion of disulfide bonding information, as described by Cooke et al. (1992). The deviation of the average S−S distance from the ideal bond length (2.02 Å) for the 15 possible cysteine pairings was used to determine which single disulfide pattern was favored. The pairing 3−15, 4−20, and 10−21 produced the lowest rms deviation from ideal S−S distance averaged over all bridges in all structures, and in all of the 20 structures this pattern gave the lowest rmsd from ideal S−S distances (supporting information, Table S3). In conclusion, the pattern of disulfide bridges determined from the NMR data is consistent with that proposed for the natural toxin (Hidaka et al., 1990).

Structure Determination. Initial structures were based on 289 interproton distance restraints derived from 177 intraresidual, 64 sequential, and 48 medium- and long-range NOEs. These restraints were checked for violations, and ambiguous cross peaks were resolved prior to the calculation of a further 50 structures with the addition of 9 backbone and 5 side chain dihedral angle restraints from spin−spin coupling constants. The 20 structures with the lowest energies were chosen to represent the solution structure of GIIIB. These structures satisfied the experimental restraints, having no interproton distance violations greater than 0.2 Å or torsion angle violations greater than 3°. A summary of the geometric and energetic statistics for the family of structures is given in Table 2. These data show well-converged structures with good stereochemistry.

Table 2: Geometric and Energetic Statistics for the 20 Final Structures of GIIIB[a]

rms deviations from experimental restraints	
interproton distances (Å) (289)[b]	0.024 ± 0.002
dihedral angles (deg) (14)[b]	0.116 ± 0.082
rms deviations from idealized geometry	
bonds (Å)	0.007 ± 0.001
angles (deg)	2.05 ± 0.03
impropers (deg)	0.17 ± 0.01
energies (kcal mol^{-1})	
E_{NOE}[c]	1.61 ± 0.28
E_{cdih}[c]	0.02 ± 0.02
$E_{L\text{-}J}$[d]	−91.4 ± 3.1
$E_{bond} + E_{angle} + E_{improper}$	41.8 ± 1.7

[a] The values in the table are the mean ± standard deviation. [b] The number of restraints is shown in parentheses. None of the structures had distance violations >0.2 Å or dihedral angle violations >3°. [c] Force constants for the calculation of square-well potentials for the NOE and dihedral angle restraints were 50 kcal mol^{-1} Å^{-1} and 200 kcal mol^{-1} rad^{-2}, respectively. [d] The Lennard-Jones van der Waals energy was calculated with the CHARMm empirical energy function.

The rms differences for the backbone atoms when the final 20 structures are superimposed over the entire molecule are shown as a function of residue number in Figure 6A. These data indicate that the structure is well defined, except for the N- and C-terminal residues, with rmsd values in the range 0.4−0.7 Å. The majority of backbone dihedral angles are well defined, having angular order parameters ≥0.95 (Figure 6B,C). Residues 9 and 10 are not as precisely defined, reflecting the small number of medium- and long-range NOEs for this region of the molecule; however, for the purpose of calculating rms differences they have been included with the well-defined residues. Excluding the N-terminal residues 1−2 and C-terminal residue 22, the mean pairwise rms differences for the backbone and all heavy atoms were 0.74 and 2.54 Å, respectively. Corresponding values for the whole molecule were 1.22 and 2.48 Å, respectively. The side chain dihedral angles χ^1 and χ^2 are not as well defined (Figure 6D,E) due to the fact that many side chains are surface exposed. However, among the best defined side chains (other than cysteine residues) are those of Arg8 and Lys9 which form the second strand of the β-hairpin.

A Ramachandran plot of the angular average of the family of 20 structures (supporting information, Figure S2A) demonstrates the high quality of the final structures by the fact that most residues occupy the favorable regions, with the exception of Asp2 and Cys10. The backbone dihedral angles of these residues are apparently poorly defined; however, in the case of Cys10 this is due to the population of two distinct and well-defined conformations (supporting information, Figure S2B) as discussed below.

Description of the Structure. Stereoviews of the 20 final structures superimposed over the backbone atoms of residues 3−21 are shown in Figure 7. The major structural features of GIIIB are a distorted helix from residues 13−22 and a small β-hairpin involving residues 3−9, having a turn

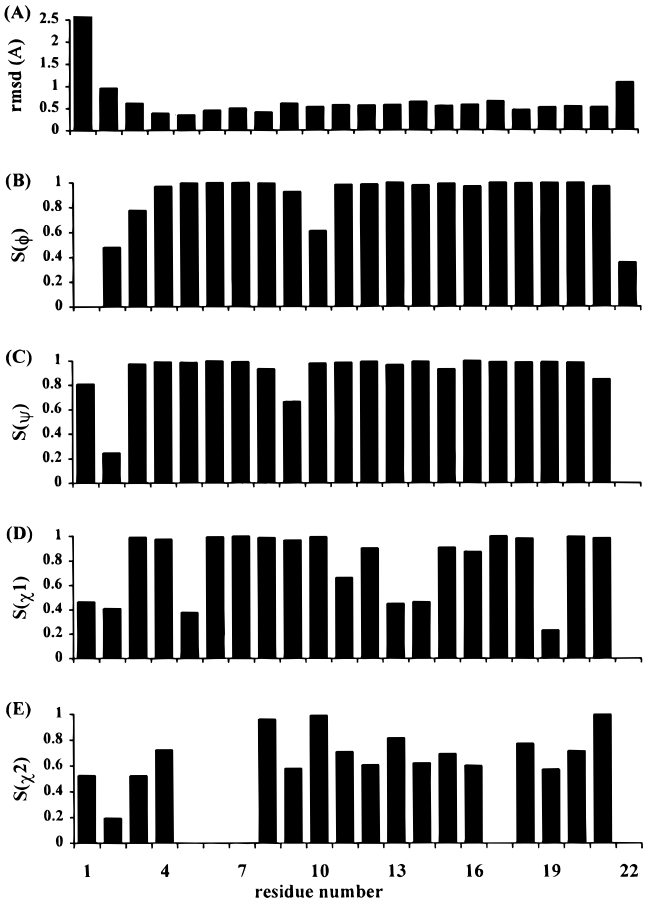

FIGURE 6: Parameters characterizing the final family of structures for GIIIB, plotted as a function of residue number: (A) rms differences from the average structure for the backbone atoms; (B−E) angular order parameters (Hyberts et al., 1992; Pallaghy et al., 1993) for the backbone dihedral angles ϕ and ψ and the side chain angles χ^1 and χ^2.

centered around residues 6−7. The helix and β-hairpin are joined by two disulfide bonds, Cys3−Cys15 and Cys4−Cys20. A third disulfide bond, Cys10−Cys21, is also located near the helix and β-hairpin.

Several turns in the peptide were identified using the standard criterion that $C\alpha_i$ is less than 7 Å from $C\alpha_{i+3}$ (Lewis et al., 1973) and by the characteristic distance connectivities of the backbone protons (Wüthrich, 1976). It is convenient to describe these in terms of the nomenclature introduced by Wilmot and Thornton (1990). One of the turns involves residues 2−5. The average ϕ, ψ angles for Cys3 and Cys4 are −104°, −53° and −89°, −3°, respectively, and therefore this turn may be classified as $\alpha\alpha$ type (Wilmot & Thornton, 1990), i.e., equivalent to a type I β-turn in the more traditional nomenclature. The amide NH proton of Thr5 exchanges slowly; however, the expected hydrogen bond to the Asp2 carbonyl oxygen is formed in only two of the final structures. As the central residues of this turn are cysteines which participate in disulfide bonds and exhibit a number of long-range Hα−Hα and Hα−NH NOEs consistent with them also being in a small β-hairpin (Figure 5), distortion in this region of the structure is not unexpected. A second turn involving residues 5−8 reverses the direction of the backbone between the two strands in the β-hairpin. These residues are well defined, both in terms of average backbone rmsd and angular order parameters (Figure 6), but do not match any of the established turn types. The deviation from a standard turn structure reflects the presence of a *trans*-hydroxyproline at position 6 and a *cis*-hydroxyproline at position 7. The average ϕ, ψ dihedral angles for Hyp6 and Hyp7 are −62°, 136° and −70°, 137°, respectively, and therefore the turn may be described as $\beta_P\beta_P^{cis-Hyp}$. A third turn involving residues 9−12 joins the β-hairpin to the helix. The average ϕ, ψ angles for Cys10 and Lys11 are −61°, 11° and −84°, −30°, respectively, and therefore the turn may, in principle, be classified as $\alpha\alpha$ or type I. However, this region is poorly defined and cannot be precisely characterized. Low angular order parameters (Figure 6) suggest that the turn involving residues 9−12 accesses more than one conformation. This was confirmed by examination of the Ramachandran plots for these residues. A Ramachandran plot for Cys10 in the 20 final structures is shown in the supporting information (Figure S2B). This region in the calculated structures appears to be represented by two conformations: either a $\alpha\alpha$ type turn (with Asp12 NH−Lys9 CO hydrogen bond; 6 structures) or a distorted turn (14 structures) that does not match any of the established types with ϕ, ψ angles for Cys10 and Lys11 in the α_L and α_R regions of the Ramachandran plot, respectively. This feature of the calculations could result from the small number of NOE restraints for this region and should not necessarily be taken as evidence of multiple conformations. However, the broadening of the Cys10 NH proton resonance as a function of temperature strongly supports the suggestion of interconversion between two or more local conformations. Examination of the structures shows that a flip between the proposed conformations could readily occur in this localized region without disrupting the global fold.

The hydrogen bonds present in the final structures (Table 3) adequately explain the observed slowly exchanging amide protons, with the exceptions being the backbone amides of Thr5 and Asp12. These results indicate that the carbonyl oxygen atoms of residues 12−19 favor the i, $i+3$ hydrogen bonds observed in 3_{10}-helices over the i, $i+4$ hydrogen bonds observed in regular α-helices, suggesting that 3_{10}-helix is the dominant folded form in the structural equilibrium. The hydrogen-bonding pattern of the helix is, however, interrupted by the side chain of Hyp17.

The structure of GIIIB is stabilized by three disulfide bonds (3−15, 4−20, and 10−21). The conformation of the disulfide bonds is well defined (Figures 6 and 7), and the torsion angles of the Cys3−Cys15 and Cys10−Cys21 disulfide bonds are representative of a left-handed spiral (Richardson, 1981; Srinivasan et al., 1990). The conformation of the Cys4−Cys20 disulfide bond also has a χ^3 angle of −90°, but the combination of side chain dihedral angles does not fit any of the classifications of Srinavasan et al. (1990).

DISCUSSION

General Features of the GIIIB Structure. In the present study, we have determined the three-dimensional structure of μ-conotoxin GIIIB in aqueous solution using 2D ^{1}H NMR spectroscopy and simulated annealing calculations. The structure is composed of a small β-hairpin involving residues 3−9, a 3_{10}-helix from residues 13−22, and several turns. In addition, there are three disulfide bonds and a number of intramolecular hydrogen bonds, resulting in a compact and well-defined structure. Many of the secondary structure

FIGURE 7: Stereoviews of the 20 final structures of GIIIB superimposed over the backbone atoms of residues 3−21. The three disulfide bonds are shown in lighter shading.

Table 3: Hydrogen Bond Statistics for Slowly Exchanging Amide Protons in GIIIB

secondary structure	donor	acceptor	occurrence[a]
β-turn	Thr5 NH	Asp2 CO	2
β-hairpin	Lys9 NH	Cys3 CO	17
β-turn	Asp12 NH	Lys9 CO	6
3_{10}-helix	Cys15 NH	Asp12 CO	17
	Lys16 NH	Asp12 CO	13
	Lys16 NH	Arg13 CO	6
	Met18 NH	Arg14 CO	3
	Met18 NH	Cys15 CO	4
	Cys21 NH	Met18 CO	18
	Ala22 NH	Met18 CO	13
	Ala22 NH	Lys19 CO	7

[a] Analysis of 20 final structures generated without hydrogen bond restraints. Hydrogen bonds were identified according to the criteria of Kabsch and Sander (1983).

elements are distorted; however, this is not unexpected considering the small size and high disulfide content of the molecule. Aside from these distortions, it is interesting that such a small molecule is able to adopt a well-defined three-dimensional structure exhibiting characteristics of a protein.

Important characteristics of the μ-conotoxins from *C. geographus* include the presence of three hydroxyproline residues and a large number (40−45%) of charged residues as shown in Figure 1. In GIIIB, Hyp6 and Hyp7 are the central positions of a tight turn between the two strands in the β-hairpin, and Hyp17 is in the helical region of the structure. The conformations of the peptide bonds preceding Hyp6, Hyp7, and Hyp17 were determined to be *trans*, *cis*, and *trans*, respectively, using a combination of sequential NOE connectivities and ^{13}C chemical shift information. In previous studies of the related peptide GIIIA by ^{1}H NMR spectroscopy (Lancelin et al., 1991; Ott et al., 1991; Wakamatsu et al., 1992), a *cis* peptide bond conformation for Hyp7 was suggested but not experimentally verified due to chemical shift degeneracy of the Hα protons of Hyp6 and Hyp7. ^{13}C chemical shifts have previously been used in conjunction with sequential NOE connectivities to identify the conformation of proline residues [for recent examples, see Archer et al. (1993), Chandrasekhar et al. (1994), and Toy-Palmer et al. (1995)]. In the case of a *trans*-proline peptide bond conformation, the chemical shift dispersion of Cβ and Cγ is ~5 ppm, while a *cis*-proline shows significantly greater chemical shift dispersion ($\Delta\delta_{C\beta-C\gamma} \cong 10$ ppm) (Wüthrich et al., 1972). By contrast to proline, for hydroxyproline, an increased ^{13}C chemical shift dispersion of Cγ and Cβ indicates that the preceding carbonyl is configured in a *trans* peptide bond ($\Delta\delta_{C\gamma-C\beta} \cong 33$ ppm), while for *cis*-hydroxyproline the corresponding value is ~30 ppm. This is illustrated for the hydroxyproline residues of GIIIB in Table 1. Hydroxyproline residues are not common in many families of peptides; however, they are highly prevalent in conotoxins. Hence, ^{13}C chemical shifts in combination with sequential NOE connectivities should be a valuable aid in determining the conformation of hydroxyproline residues in other conotoxins.

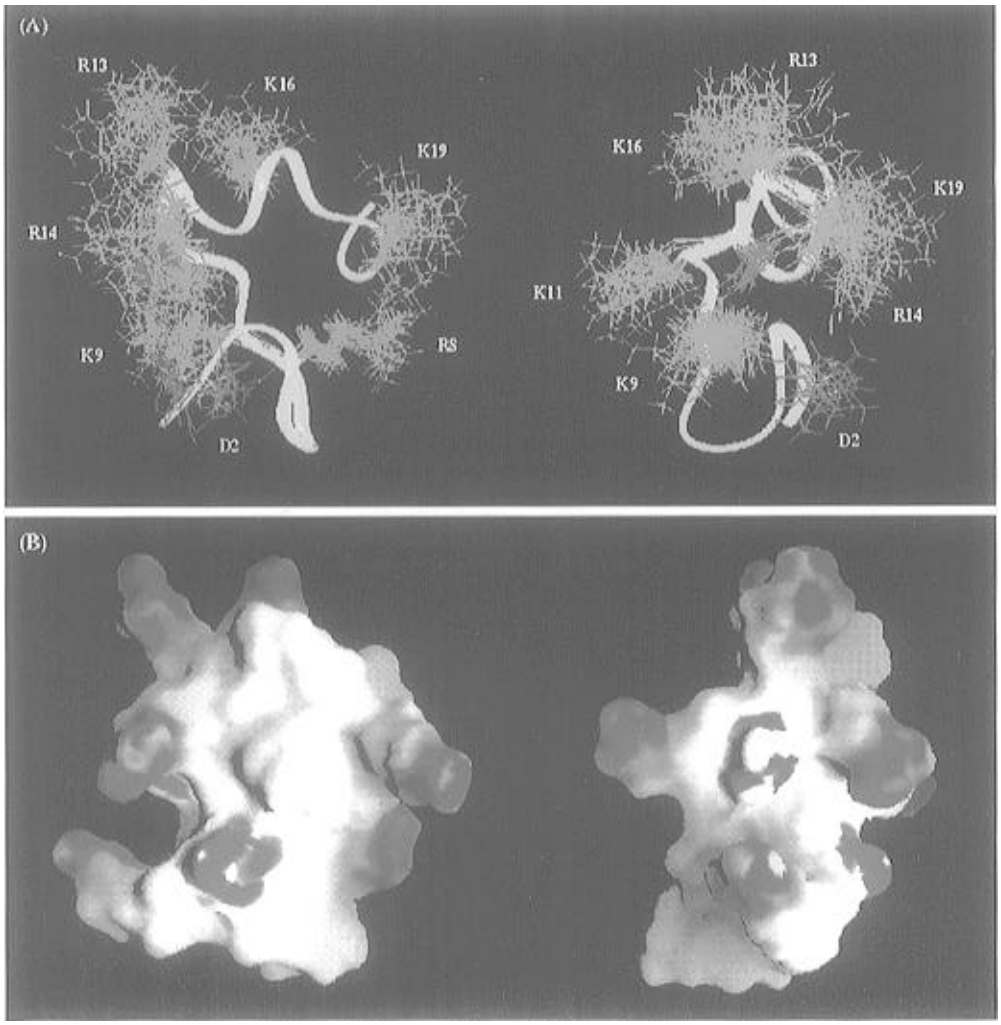

FIGURE 8: Location of the charged amino acid side chains in GIIIB presented in two different orientations. The second view is related to the first by a rotation of 90° about the vertical axis. (A) Side chains of residues Asp2, Arg8, Lys9, Lys11, Asp12, Arg13, Arg14, Lys16, and Lys19 for 20 structures are shown. Positively and negatively charged side chains are colored blue and magenta, respectively. The backbone of the lowest energy structure is represented by a ribbon, and the side chain of Arg1 has been omitted for clarity. (B) A surface representation of the lowest energy structure generated with a probe radius of 1.4 Å is shown. Surface-associated electrostatic potentials are represented from electronegative to electropositive by a red to blue continuous color range. The diagram was generated using GRASP (Nicholls et al., 1991).

A consequence of the global fold of GIIIB is the spatial distribution of the different charged side chains. As mentioned previously, there is a large number of exposed residues, most of which bear formally charged groups. This toxin contains eight positively (Arg1, Arg8, Lys9, Lys11, Arg13, Arg14, Lys16 and Lys19) and two negatively charged residues (Asp2 and Asp12). Four of these, i.e., Arg13, Arg14, Lys16, and Lys19, are located in the helix, and four others, Arg8, Lys9, Lys11, and Asp12, are in the β-hairpin and the region linking the helix to the hairpin. The location of the charged side chains is illustrated in Figure 8. These side chains project into the solvent in a radial orientation relative to the core of the molecule and form potential sites of interaction with anionic sites (Noda et al., 1989; Terlau et al., 1991) on the sodium channels. As is common for surface-exposed arginines and lysines, they are poorly defined, with the exception of Arg8 and Lys9 (Figures 6 and 8A). The mobility of these side chains may facilitate the initial interactions between the toxin and the skeletal muscle sodium channel. Despite the large number of possible orientations of these side chains, an upper estimate of the distance between each cationic site of 20−25 Å can be made. A functional map of the molecular surface of charybdotoxin, a 37-residue polypeptide from the scorpion *Leiurus quinquestriatus hebraeus* which targets many types of potassium channels, has identified a complementary receptor site which has a similar 20−25 Å diameter (Bontems et al., 1992). For μ-conotoxins and charybdotoxin, a compact structural core presents the interactive solvent-exposed amino acid side chains in the appropriate topology for binding (Lancelin et al., 1994). Interestingly, these toxins also possess a similar backbone fold as discussed below.

Comparison with μ-Conotoxin GIIIA. A major aim of this study was to compare the structure of GIIIB with that of the related μ-conotoxin GIIIA to determine the effect of amino acid substitutions on the conformation. This information in combination with structure−activity data should provide further insight into the interaction of the μ-conotoxins with skeletal muscle sodium channels.

Information on the structural differences between peptides can be obtained from chemical shifts, which are sensitive indicators of local conformations. Chemical shift changes for the backbone Hα and NH protons of GIIIB and GIIIA (Wakamatsu et al., 1992), other than the expected differences near the substituted residues, are small ($\leq$0.1 ppm), suggesting that the backbone conformation of the peptides is

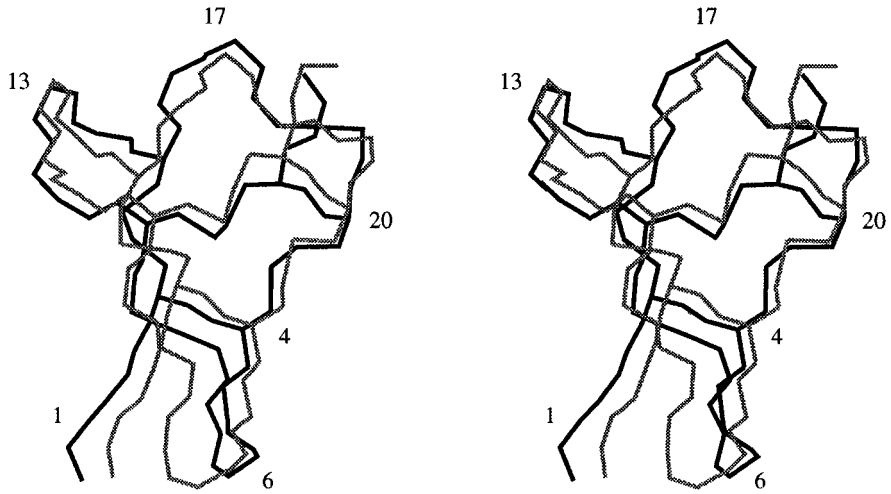

FIGURE 9: Superimposition of GIIIB (darker line) and GIIIA over the backbone heavy atoms (N, Cα, C) of the entire molecule. The coordinates for GIIIA were obtained from the Brookhaven Protein Data Bank (code 1TCG).

essentially identical. This is supported by similar $^3J_{NH-H\alpha}$ coupling constants and slowly exchanging backbone amide protons. The observation of similar sequential and medium-range NOEs also suggests that the secondary structural features of the two peptides are the same. However, several $H\alpha-NH_{i+3}$ and $H\alpha-H\beta_{i+3}$ connectivities indicative of helix were present for the Arg13−Ala22 segment of GIIIB. NOE connectivities characteristic of helix were not observed for the corresponding region in GIIIA (Lancelin et al., 1991; Ott et al., 1991; Wakamatsu et al., 1992).

The three-dimensional structure of GIIIA has previously been determined using 2D ^{1}H NMR (Lancelin et al., 1991; Ott et al., 1991; Wakamatsu et al., 1992) and consists of β-turns (Asp2−Thr5 and Thr5−Lys8), a linear extension (Lys8−Asp12), a non-hydrogen-bonded loop (Asp12−Cys15), and a single right-handed helical turn (Cys15−Gln18), with a final loop directing the C-terminus away from the core in the opposite direction to the N-terminus. These studies of GIIIA are in general agreement, except that where one (Ott et al., 1991) finds less structured coil between residues 15−18, the others show one turn of helix (Lancelin et al., 1991; Wakamatsu et al., 1992). By contrast, the results obtained in the current study indicate that the secondary structure of GIIIB includes a small β-hairpin involving residues 3−9 and 3_{10}-helix from residues 13−22.

The overall fold of GIIIB is essentially the same as that previously determined for GIIIA (Wakamatsu et al., 1992), the backbone atoms of the entire molecule superimposing with an average rms difference of 1.36 Å. The backbone superimposition of GIIIB and GIIIA displayed in Figure 9 illustrates the structural similarity of these toxins. First, the β-hairpin region of the two structures (residues 3−9) is very similar with an average rms difference of 0.67 Å for the backbone atoms. A β-hairpin in this region was not reported for GIIIA; however, our examination of the coordinates and analysis of the structures indicate that it is present. Furthermore, characteristic $d_{\alpha\alpha}(4,8)$ and $d_{\alpha N}(3,9)$ NOEs for this element of secondary structure were reported for GIIIA (Lancelin et al., 1991), and inspection of the mean structure also indicates the presence of the interstrand Lys9 NH−Cys3 CO hydrogen bond. Second, the helix in GIIIB involves residues 13−22 by contrast to the single turn of helix (15−18) reported for GIIIA (Lancelin et al., 1991; Wakamatsu et al., 1992). The hydrogen bonds observed for the 3_{10}-helix in GIIIB adequately explain the slowly exchanging amide NH protons, whereas in the study of GIIIA (Lancelin et al., 1991) no explanation for the slowly exchanging amide NH proton of Ala22 was provided, and those of Lys16, Met18, and Cys21 could only be rationalized with distortions on N−O distances or N−H−O angles. The better definition in this region of the structure of GIIIB compared with GIIIA may reflect the larger number of distance restraints for GIIIB.

In summary, GIIIB and GIIIA have a common global fold (Figure 9) and are also similar at the level of their local backbone conformations. As the sequences of GIIIB and GIIIA differ by only four residues, it is not surprising that their secondary structures are similar. Differences between the reported structure of GIIIA (Lancelin et al., 1991; Ott et al., 1991; Wakamatsu et al., 1992) and that determined for GIIIB in this study appear to reflect differences in the number of distance restraints and in interpretation rather than major structural changes.

Structure−Activity Relationships of μ-Conotoxins. The best characterized μ-conotoxins, GIIIA and GIIIB, exhibit strong selectivity between sodium channel subtypes. Both toxins bind with nanomolar affinity to the skeletal muscle and eel electroplax sodium channels but exhibit little affinity for neuronal and cardiac channel subtypes (Cruz et al., 1985; Moczydlowski et al., 1986; Ohizumi et al., 1986; Chen et al., 1992). GIIIA and GIIIB have similar biological activity profiles; however, one study (Sato et al., 1983) has suggested that the guanidino group at residue 14 in GIIIB enhances its biological activity relative to GIIIA (ip LD_{50} in mice of GIIIB and GIIIA are 110 and 340 μg/kg, respectively). The roles of various residues in GIIIA have been examined by chemical modification studies (Sato et al., 1991; Becker et al., 1992); however, there are no reports of the specific amino acids in GIIIB that are required for biological activity. Studies of GIIIA suggest that amino acid residues sensitive to replacement by alanine are Arg13 > Arg19 > Hyp17 > Lys16 > Arg1 > Lys8, with the extent of activity loss in this order (Sato et al., 1991). The basicity of the molecule is a crucial factor for activity, with mutations of Arg13 having the largest single effect on binding affinity (Sato et al., 1991; Becker et al., 1992). This implies that a guanidinium group is required for block of the channel, as is the case with the neurotoxins TTX and STX [for review see Kao (1986)]. However, the interaction appears to be complex, with a

number of residues significantly contributing to the potency of the native toxin. Certain residues are important primarily in the approach and docking of the peptide with the channel site (Lys11 and Arg19), while others are important for strength of binding once the toxin has attached (Hyp17 and Arg1) (Becker et al., 1992). The binding site is rather wide, consistent with the macrosite model of Olivera et al. (1991), allowing multiple interactions between the toxin molecule and the sodium channel. Effects of amino acid substitutions may therefore be compensated by the binding of other side chains, and potentially a large number of diverse peptide structures could bind different subsets of microsites within the same macrosite.

Several residues important for the activity of GIIIA are conserved in GIIIB (i.e., Arg13, Lys16, and Hyp17), suggesting that these residues are also likely to be involved in binding of GIIIB to the sodium channel. These residues are located in the 3_{10}-helix and clearly reside on one side of the molecule (Figure 8). The corresponding face of GIIIA has been suggested to interact with the sodium channel (Wakamatsu et al., 1992), and the helix provides an efficient way of presenting the side chains to be recognized by the receptor site. Another important residue for the activity of GIIIA, Arg19, is replaced by lysine at this position in GIIIB. Mutagenesis of GIIIA has shown that Arg19 can be replaced by Lys without significant loss of activity (Becker et al., 1992), implying that conservation of a positive charge at this position is sufficient. In addition, the extra positively charged residue in GIIIB relative to GIIIA, Arg14, is located in the helix and oriented so that it may also interact with the sodium channel. The role of this extra positive charge in GIIIB or the effect of a Q14R substitution on the potency of GIIIA has not been studied. However, the suggestion that the guanidino group at position 14 enhances its activity relative to GIIIA and the fact that the basicity, especially around residue 13, is important for the activity of GIIIA make it worthy of further investigation.

An additional benefit of studying these peptides is that the current methods available for atomic resolution structural analysis of biomolecules are not amenable to the study of ion channels directly. Understanding how the topology of rigid peptide ligands determines their interaction with the channel provides an indirect view of the ion channel itself and answers important questions regarding the molecular basis for binding and selectivity (Reily et al., 1995). While GIIIB cannot be regarded as a completely rigid ligand due to evidence suggesting multiple conformations near Cys10 and flexibility of the side chains, its basic fold is well defined. The size of the μ-conotoxins and the broad distribution of residues that contribute to the toxin−channel interactions provide valuable information regarding structural and functional models of the pore region of the sodium channel. Dudley et al. (1995) have recently described a mutation E758Q in the outer vestibule region of the skeletal muscle sodium channel that decreased the binding affinity of GIIIA by 48-fold. Using this information and their previous model of the TTX and STX binding site (Lipkind & Fozzard, 1994), they have proposed a model for GIIIA block of the sodium channel. The model involves the interaction of the guanidinium group of R13 with a triad of carboxyl groups in the outer vestibule (D400, E755, and E758). However, at present this model does not explain the strong preference of GIIIA for skeletal muscle and electric eel organ sodium channels.

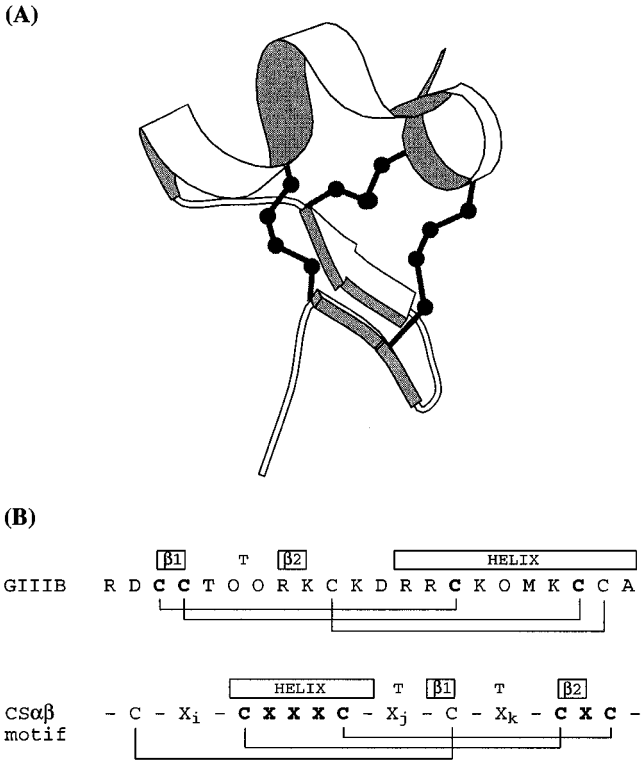

FIGURE 10: (A) Richardson-style diagram of the backbone of the lowest energy structure of GIIIB, showing the β-sheet (arrows), the 3_{10}-helix (coil), and the disulfide bonds. The diagram was generated using MOLSCRIPT (Kraulis, 1991). (B) Schematic representation of the secondary structural elements of GIIIB and the cysteine-stabilized $\alpha\beta$ (CS$\alpha\beta$) motif. β-Strands and helices are indicated by a rectangle and turns by the letter T. The disulfide connectivities are shown by horizontal lines. In the CS$\alpha\beta$ motif (Cornet et al., 1995), the helical conformation of the sequence C-X-X-X-C is stabilized by disulfide bonds to the sequence C-X-C in a β-strand. These residues are in bold type. Other elements of secondary structure can be summarized as follows: X_i corresponds to an N-terminal loop; X_j to the end of the helix, the first β-strand, and the turn between them; and X_k to the turn between the two β-strands.

Comparison of the structure of GIIIB and the model for GIIIA block of the sodium channel suggests that Arg14 may also be in close proximity to E758 in the outer vestibule. The structure of GIIIB determined in this study provides the basis for further understanding of the structure−activity relationships of the μ-conotoxins and for their binding to skeletal muscle sodium channels. As the database of neurotoxin structures increases and further information on amino acid residues forming the receptor site of sodium channels is obtained from site-directed mutagenesis and expression of mutant sodium channel cDNAs, we will be better able to answer questions regarding sodium channel structure and the binding specificity of these compounds.

Comparison with Other Polypeptide Structures. As previously mentioned, one characteristic feature of GIIIB is the stabilization of its structure by disulfide bonds. A MOLSCRIPT representation of the secondary structure and disulfide bonds is shown in Figure 10A. Two of the three disulfide bonds present connect the helix and the β-sheet, forming a structural core with similarities to the "cysteine-stabilized $\alpha\beta$" (CS$\alpha\beta$) motif (Cornet et al., 1995). In this motif, the helical conformation of the sequence Cys-X-X-X-Cys is stabilized by disulfide bonds to the sequence Cys-X-Cys in a β-strand. The helix and strand run in the same

direction, and they are separated in the sequence by a stretch of residues forming another β-strand in the opposite direction. Figure 10B summarizes the secondary structural elements of the CS$\alpha\beta$ motif and those determined for GIIIB in this study. The same features are present in GIIIB; however, the helix is connected to a parallel strand which precedes it in the sequence. There are also differences in the spacing between the cysteine residues, with four residues between cysteines in the helical region and no residue separating cysteine residues in the β-sheet of GIIIB (Figure 10B).

Similar motifs in which the β-sheet can involve two or three strands are present in several families of small proteins (30−70 residues) from diverse biological sources. These include (i) all known structures of scorpion toxins, irrespective of their size, amino acid sequence, and function (Bontems et al., 1991a,b; Johnson et al., 1994; Lippens et al., 1995; Krezel et al., 1995), (ii) insect defensins (Bonmatin et al., 1992; Cornet et al., 1995), and (iii) plant γ-thionins (Bruix et al., 1993). The occurrence of this motif in polypeptides with very different activities and unrelated amino acid sequences suggests that it is an energetically favorable and stable structural element. The consensus pattern has also been found in apamin, a neurotoxin from honey bee venom (Pease & Wemmer, 1988), where the corresponding motif was named the "cysteine-stabilised α-helix" (CSH) (Tamaoki et al., 1991; Kobayashi et al., 1991). As for GIIIB, the helix in apamin is connected to a parallel strand which precedes it in the sequence. A similar motif has also been observed in two small peptides with vasoconstricting activity, human endothelin and snake venom sarafotoxin (Kobayashi et al., 1991). However, in these compounds the helix and β-strand have opposite directions.

As the CS$\alpha\beta$ motif contains most of the secondary structural elements found in protein structures, it has been proposed as a scaffold for protein engineering (Vita et al., 1995) upon which new sequences can be transferred, a specific conformation can be reproduced, and tailored functions can be generated. This motif is amenable to chemical synthesis due to its small size, is highly stable, and tolerates multiple sequence mutations. For example, Vita et al. (1995) have recently engineered the Zn^{2+} binding site of carbonic anhydrase B onto the scaffold of charybdotoxin. The high sequence permissiveness of the CS$\alpha\beta$ motif suggests that any region can be engineered with new sequences, thus making it an ideal scaffold for production of conformationally constrained peptide libraries (Vita et al., 1995). The possibility of using the natural scaffold of small disulfide stabilized structures for peptide libraries has previously been proposed for conotoxins (Olivera et al., 1990, 1991, 1995). Probably, many more functions than those naturally selected could be artificially engineered on these structurally stable templates.

ACKNOWLEDGMENT

We thank David Smith for the program SSTRUC, Kathy Nielsen and Martin Scanlon for helpful discussions and assistance with computing, and Jon-Paul Bingham for comparing the synthetic GIIIB with the natural toxin.

SUPPORTING INFORMATION AVAILABLE

Tables of ^{1}H resonance assignments, ^{13}C resonance assignments, and statistical analysis of the possible disulfide bonding patterns in GIIIB and figures showing the aliphatic Cα−Hα region of the HMQC spectrum and Ramachandran plots for (A) the angular average and (B) Cys10 for the 20 final structures (5 pages). Ordering information is given on any current masthead page.

REFERENCES

Archer, S. J., Bax, A., Roberts, A. B., Sporn, M. B., Ogawa, Y., Piez, K. A., Weatherbee, J. A., Tsang, M. L.-S., Lucas, R., Zheng, B.-L., Wenker, J., & Torchia, D. A. (1993) *Biochemistry 32*, 1164−1171.

Bax, A., & Davis, D. G. (1985) *J. Magn. Reson. 65*, 355−360.

Bax, A., Griffey, R. H., & Hawkins, B. L. (1983) *J. Magn. Reson. 55*, 301−315.

Becker, S., Prusak-Sochaczewski, E., Zamponi, G., Beck-Sickinger, A. G., Gordon, R. G., & French, R. J. (1992) *Biochemistry 31*, 8229−8238.

Bonmatin, J. M., Bonnat, J. C., Gallet, X., Vovelle, F., Ptak, M., Reichhart, J. M., Hoffmann, J. A., Keppi, E., Legrain, M., & Achstetter, T. (1992) *J. Biomol. NMR 2*, 235−256.

Bontems, F., Roumestand, C., Boyot, P., Gilquin, B., Doljansky, Y., Ménez, A., & Toma, F. (1991a) *Eur. J. Biochem. 196*, 19−28.

Bontems, F., Roumestand, C., Gilquin, B., Ménez, A., & Toma, F. (1991b) *Science 254*, 1521−1523.

Bontems, F., Gilquin, B., Roumestand, C., Ménez, A., & Toma, F. (1992) *Biochemistry 31*, 7756−7764.

Braunschweiler, L., & Ernst, R. R. (1983) *J. Magn. Reson. 53*, 521−528.

Brooks, B. R., Bruccoleri, R. E., Olafson, B. D., States, D. J., Swaminathan, S., & Karplus, M. (1983) *J. Comput. Chem. 4*, 187−217.

Bruix, M., Jiménez, M. A., Santoro, J., González, C., Colilla, F. J., Méndez, E., & Rico, M. (1993) *Biochemistry 32*, 715−724.

Brünger, A. T. (1992) *X-PLOR Manual Version 3.1*, Yale University, New Haven, CT.

Catterall, W. A. (1988) *Science 242*, 50−61.

Catterall, W. A. (1995) *Annu. Rev. Biochem. 64*, 493−531.

Chandrasekhar, K., Campbell, A. P., Jeng, M.-F., Holmgren, A., & Dyson, H. J. (1994) *J. Biomol. NMR 4*, 411−432.

Chen, L.-Q., Chahine, M., Kallen, R. G., Barchi, R. L., & Horn, R. (1992) *FEBS Lett. 309*, 253−257.

Clore, G. M., Nilges, M., Sukuraman, D. K., Brünger, A. T., Karplus, M., & Gronenborn, A. M. (1986a) *EMBO J. 5*, 2729−2735.

Clore, G. M., Brünger, A. T., Karplus, M., & Gronenborn, A. M. (1986b) *J. Mol. Biol. 191*, 523−551.

Cooke, R. M., Carter, B. G., Murray-Rust, P., Hartshorn, M. J., Herzyk, P., & Hubbard, R. E. (1992) *Protein Eng. 5*, 473−477.

Cornet, B., Bonmatin, J.-M., Hetru, C., Hoffmann, J. A., Ptak, M., & Vovelle, F. (1995) *Structure 3*, 435−448.

Cruz, L. J., Gray, W. R., Olivera, B. M., Zeikus, R. D., Kerr, L., Yoshikami, D., & Moczydlowski, E. (1985) *J. Biol. Chem. 260*, 9280−9288.

Dudley, S. C., Todt, H., Lipkind, G., & Fozzard, H. A. (1995) *Biophys. J. 69*, 1657−1665.

Garbay-Jaureguiberry, C., Arnoux, B., Prangé, T., Wehri-Altenburger, S., Pascard, C., & Roques, B. P. (1980) *J. Am. Chem. Soc. 102*, 1827−1837.

Griesinger, C., Sørensen, O. W., & Ernst, R. R. (1987) *J. Magn. Reson. 75*, 474−492.

Hidaka, Y., Sato, K., Nakamura, H., Kobayashi, J., Ohizumi, Y., & Shimonishi, Y. (1990) *FEBS Lett. 264*, 29−32.

Howarth, O. W., & Lilley, D. M. J. (1978) *Prog. NMR Spectrosc. 12*, 1−40.

Hyberts, S. G., Marki, W., & Wagner, G. (1987) *Eur. J. Biochem. 164*, 625−635.

Hyberts, S. G., Golberg, M. S., Havel, T. S., & Wagner, G. (1992) *Protein Sci. 1*, 736−751.

Jeener, J., Meier, B. H., Bachmann, P., & Ernst, R. R. (1979) *J. Chem. Phys. 71*, 4546−4553.

Johnson, B. A., Stevens, S. P., & Williamson, J. M. (1994) *Biochemistry 33*, 15061−15070.

Kabsch, W., & Sander, C. (1983) *Biopolymers 22*, 2577−2637.

Kallen, R. G., Cohen, S. A., & Barchi, R. L. (1993) *Mol. Neurobiol. 7*, 383−428.
Kao, C. Y. (1986) *Ann. N.Y. Acad. Sci. 479*, 52−67.
Klaus, W., Broger, C., Gerber, P., & Senn, H. (1993) *J. Mol. Biol. 232*, 897−906.
Kobayashi, Y., Takashima, H., Tamaoki, H., Kyogoku, Y., Lambert, P., Kuroda, H., Chino, N., Watanabe, T. X., Kimura, T., Sakakibara, S., & Moroder, L. (1991) *Biopolymers 31*, 1213−1220.
Kraulis, P. (1991) *J. Appl. Crystallogr. 24*, 946−950.
Krezel, A. J., Chandrasekhar, K., Hidalgo, P., MacKinnon, R., & Wagner, G. (1995) *Protein Sci. 4*, 1478−1489.
Lancelin, J.-M., Kohda, D., Tate, S., Yanagawa, Y., Abe, T., Satake, M., & Inagaki, F. (1991) *Biochemistry 30*, 6908−6916.
Lancelin, J.-M., Foray, M.-F., Poncin, M., Hollecker, M., & Marion, D. (1994) *Nat. Struct. Biol. 1*, 246−250.
Lerner, L., & Bax, A. (1986) *J. Magn. Reson. 69*, 375−380.
Lewis, P. N., Momany, F. A., & Scheraga, H. A. (1973) *Biochim. Biophys. Acta 303*, 211−229.
Lipkind, G. M., & Fozzard, H. A. (1994) *Biophys. J. 66*, 1−13.
Lippens, G., Najib, J., Wodak, S. J., & Tartar, A. (1995) *Biochemistry 34*, 13−21.
Marion, D., & Wüthrich, K. (1983) *Biochem. Biophys. Res. Commun. 113*, 967−974.
Moczydlowski, E., Olivera, B. M., Gray, W. R., & Strichartz, G. R. (1986) *Proc. Natl. Acad. Sci. U.S.A. 83*, 5321−5325.
Myers, R. A., Cruz, L. J., Rivier, J. E., & Olivera, B. M. (1993) *Chem. Rev. 93*, 1923−1936.
Nicholls, A., Sharp, K. A., & Honig, B. (1991) *Proteins: Struct., Funct., Genet. 11*, 281−296.
Nilges, M., Gronenborn, A. M., Brünger, A. T., & Clore, G. M. (1988) *Protein Eng. 2*, 27−38.
Noda, M., Suzuki, H., Numa, S., & Stühmer, W. (1989) *FEBS Lett. 259*, 213−216.
Ohizumi, Y., Nakamura, H., Kobayashi, J., & Catterall, W. A. (1986) *J. Biol. Chem. 261*, 6149−6152.
Olivera, B. M., Rivier, J., Clark, C., Ramilo, C. A., Corpuz, G. P., Abogadie, F. C., Mena, E. E., Woodward, S. R., Hillyard, D. R., & Cruz, L. J. (1990) *Science 249*, 257−263.
Olivera, B. M., Rivier, J., Scott, J. K., Hillyard, D. R., & Cruz, L. J. (1991) *J. Biol. Chem. 266*, 22067−22070.
Olivera, B. M., Hillyard, D. R., Marsh, M., & Yoshikami, D. (1995) *Trends Biotechnol. 13*, 422−426.
Ott, K.-H., Becker, S., Gordon, R. D., & Rüterjans, H. (1991) *FEBS Lett. 278*, 160−166.
Pallaghy, P. K., Duggan B. M., Pennington, M. W., & Norton, R. S. (1993) *J. Mol. Biol. 234*, 405−420.
Pardi, A., Billeter, M., & Wüthrich, K. (1984) *J. Mol. Biol. 180*, 741−751.
Pease, J. H. B., & Wemmer, D. E. (1988) *Biochemistry 27*, 8491−8498.
Piotto, M., Saudek, V., & Sklenar, V. (1992) *J. Biomol. NMR 2*, 661−665.
Rance, M., Sørenson, O. W., Bodenhausen, G., Wagner, G., Ernst, R. R., & Wüthrich, K. (1983) *Biochem. Biophys. Res. Commun. 117*, 479−495.
Reily, M. D., Thanabal, V., & Adams, M. E. (1995) *J. Biomol. NMR 5*, 122−132.
Richardson, J. S. (1981) *Adv. Protein Chem. 34*, 169−339.
Sato, S., Nakamura, H., Ohizumi, Y., Kobayashi, J., & Hirata, Y. (1983) *FEBS Lett. 155*, 277−280.
Sato, K., Ishida, Y., Wakamatsu, K., Kato, R., Honda, H., Ohizumi, Y., Nakamura, H., Ohya, M., Lancelin, J.-M., Kohda, D., & Inagaki, F. (1991) *J. Biol. Chem. 266*, 16989−16991.
Sibanda, B. L., Blundell, T. L., & Thornton, J. M. (1989) *J. Mol. Biol. 206*, 759−777.
Srinivasan, N., Sowdhamini, R., Ramakrishnan, C., & Balaram, P. (1990) *Int. J. Pept. Protein Res. 36*, 147−155.
Stephan, M. M., Potts, J. F., & Agnew, W. S. (1994) *J. Membr. Biol. 137*, 1−8.
Strichartz, G., Rando, T., & Wang, G. K. (1987) *Annu. Rev. Neurosci. 10*, 237−267.
Tamaoki, H., Kobayashi, Y., Nishimura, S., Ohkubo, T., Kyogoku, Y., Nakajima, K., Kumagaye, S., Kimura, T., & Sakakibara, S. (1991) *Protein Eng. 4*, 509−518.
Terlau, H., Heinemann, S. H., Stühmer, W., Pusch, M., Conti, F., Imoto, K., & Numa, S. (1991) *FEBS Lett. 293*, 93−96.
Toy-Palmer, A., Prytulla, S., & Dyson, H. J. (1995) *FEBS Lett. 365*, 35−41.
Vita, C., Roumestand, C., Toma., F., & Ménez, A. (1995) *Proc. Natl. Acad. Sci. U.S.A. 92*, 6404−6408.
Wagner, G., Braun, W., Havel, T. F., Schaumann, T., Go, N., & Wüthrich, K. (1987) *J. Mol. Biol. 196*, 611−639.
Wakamatsu, K., Kohda, D., Hatanaka, H., Lancelin, J.-M., Ishida, Y., Oya, M., Nakamura, H., Inagaki, F., & Sato, K. (1992) *Biochemistry 31*, 12577−12584.
Williamson, M. P., Havel, T. F., & Wüthrich, K. (1985) *J. Mol. Biol. 182*, 295−315.
Wilmot, C. M., & Thornton, J. M. (1990) *Protein Eng. 3*, 479−493.
Wishart, D. S., & Sykes, B. D. (1994) *J. Biomol. NMR 4*, 171−180.
Wishart, D. S., Sykes, B. D., & Richards, F. M. (1991) *J. Mol. Biol. 222*, 311−333.
Wishart, D. S., Sykes, B. D., & Richards, F. M. (1992) *Biochemistry 31*, 1647−1651.
Wüthrich, K. (1976) *NMR in Biological Research: Peptides and Proteins*, Elsevier, New York.
Wüthrich, K. (1986) *NMR of Proteins and Nucleic Acids*, Wiley-Interscience, New York.
Wüthrich, K., Tun-kyi, A., & Schwyzer, R. (1972) *FEBS Lett. 25*, 104−108.
Wüthrich, K., Billeter, M., & Braun, W. (1983) *J. Mol. Biol. 169*, 949−961.

BI960073O